This article has been accepted for publication in a future issue of this journal, but has not been fully edited. Content may change prior to final publication. Citation information: DOI 10.1109/TIE.2017.2696503, IEEE Transactions on Industrial Electronics

Synchroextracting Transform

Gang Yu, Mingjin Yu and Chuanyan Xu

***Abstract*—In this paper, we introduce a new time-frequency (TF) analysis (TFA) method to study the trend and instantaneous frequency of non-linear and non-stationary data. Our proposed method is termed the synchroextracting transform (SET), which belongs to a post-processing procedure of the short-time Fourier transform (STFT). Compared with classical TFA methods, the proposed method can generate a more energy concentrated TF representation and allow for signal reconstruction.**

The proposed SET method is inspired by the recently proposed synchrosqueezing transform (SST) and the theory of the ideal TFA. To analyze a signal, it is important to obtain the time-varying information, such as the instantaneous frequency (IF) and instantaneous amplitude. The SST is to squeeze all TF coefficients into the IF trajectory. Differ from the squeezing manner of SST, the main idea of SET is to only retain the TF information of STFT results most related to time-varying features of the signal and to remove most smeared TF energy, such that the energy concentration of the novel TF representation can be enhanced greatly. Numerical and real-world signals are employed to validate the effectiveness of the SET method.

***Index Terms*—Time-frequency analysis, synchrosqueezing transform, synchroextracting transform.**

I. INTRODUCTION

The time-frequency (TF) analysis (TFA) method is an effective tool to characterize the time-varying features of non-stationary signals, which can help us to understand this non-stationary world more clearly [1], [2]. The TFA method has been developed over many years, and classical TFA methods include the short-time Fourier transform (STFT), wavelet transform and Wigner-Ville distribution [3]. However, restricted by the Heisenberg uncertainty principle or unexpected cross-terms, the classical methods suffer from low TF resolution, which leads to them not being able to characterize the non-linear behaviors of non-stationary signals precisely. Recently, some advanced post-processing methods have been proposed, such as the reassignment method (RS) [4], [5], synchrosqueezing transform (SST) [6]-[8], parametric TFA (PTFA) method [9]-[12] and demodulated TFA (DTFA) method [7], [13]. Generally, each of the proposed methods is towards to resolve one question, i.e., how to improve the TF resolution as high as possible. The eventual goal is to achieve the ideal TFA (ITFA) [14] as

$$ITFA(t,\omega) = A(t)\cdot\delta(\omega-\varphi'(t)) \tag{1}$$

which is based on a non-stationary signal model as

$$s(t) = A(t)\cdot e^{i\varphi(t)} \tag{2}$$

where $A(t)$ is the instantaneous amplitude (IA), $\varphi(t)$ denotes the instantaneous phase and its one-order derivative $\varphi'(t)$ is the instantaneous frequency (IF). The expression (1) denotes that the signal energy of ITFA should only appear in the IF trajectory. For a mono-component signal, the phase can be obtained by the Hilbert transform, but it will fail to tackle multi-component signals. A multi-component signal can be modeled as

$$s(t) = \sum_{k=1}^{n} s_k(t) = \sum_{k=1}^{n} A_k(t)\cdot e^{i\varphi_k(t)} \tag{3}$$

whose ITFA is represented as

$$ITFA(t,\omega) = \sum_{k=1}^{n} A_k(t)\cdot\delta(\omega-\varphi'_k(t)). \tag{4}$$

According to (4), the ITFA of a multi-component signal is the superposition of ITFA of each mono-component, and it is suggested to be decomposed firstly [15], [16].

RS [4] and SST [6], [8] were developed as post-processing tools and have the ability to reassign or squeeze the TF coefficients by classical TFA methods into the IF trajectory, which are approximated to the ITFA representation. In theory, RS and SST share a similar post-processing manner. RS reassigns the TF spectrogram into the IF trajectory along the two-dimensional TF direction, and the SST squeezes the TF coefficients into the IF trajectory only in the frequency direction. Thus, RS can achieve a high TF resolution but cannot allow for signal reconstruction. SST can reconstruct the interested signals but suffers from a lower TF resolution.

PTFA [9]-[11] and DTFA [7], [13] methods are designed to improve the energy concentration of the TF result by demodulating the time-varying signal based on an extended parametric math model, such as a polynomial model or Fourier model. The demodulated procedure is iterative so that the TF energy concentration can be improved step by step. In this process, how to select the appropriate math model and how to tackle the multi-component signal are challenging and hard to solve [10]. Although the energy of PTFA or DTFA results is well-concentrated, the TF result has to be restricted by the Heisenberg uncertainty principle because it is also based on an inner product operator with the TF basis function.

Manuscript received November 11, 2016; revised February 10, 2017; accepted April 4, 2017. This work was supported in part by the National Natural Science Foundation of China under Grant 51405271 and Grant 51405272.

G. Yu is with the School of Electrical Engineering, University of Jinan, Jinan 250022, China (email: yugang2010@163.com).

M. Yu and C. Xu are with the School of Automotive Engineering, Shandong Jiaotong University, Jinan 250023, China (email: 13854163213@163.com; xcy@sdjtu.edu.cn).

Corresponding author contacts, phone: +86 150 6415 5055, e-mail: yugang2010@163.com.

In this paper, inspired by the SST method and ITFA theory, we propose a novel TFA method that can generate more energy-concentrated TF results than the RS, SST, PTFA and DTFA methods. Simultaneously, it allows for reconstructing the interested components. The rest of this paper is organized as follows. Section II details the theory of our proposed method. In Section III, two numerical signals are employed to illustrate the quantified comparison of TF results generated by different TFA methods. Experimental validations are provided in Section IV, and conclusions are drawn in Section V.

II. SYNCHROEXTRACTING TRANSFORM

A. The theory

We begin this study with STFT. The STFT expression of a function $s \in L^2(\mathbb{R})$ with respect to the real and even window $g \in L^2(\mathbb{R})$ is defined as

$$G(t,\omega) = \int_{-\infty}^{+\infty} g(u-t)\cdot s(u)\cdot e^{-i\omega u}du \tag{5}$$

where $g(u-t)$ denotes the moved window and $s(u)$ is the analyzed signal. The STFT expands a one-dimensional time-series signal into the two-dimensional time-frequency plane so that we can observe and extract the IA and IF information of the signal. However, in the time and frequency domain, the window function is of bandwidth, which results in an energy-blurred spectrogram $|G(t,\omega)|$. To explore the energy distribution of the STFT result, we first let $g_\omega(u) = g(u-t)\cdot e^{i\omega u}$. According to the Parseval's theorem, the STFT can be written as

$$\begin{aligned} &G(t,\omega) \\ &= \int_{-\infty}^{+\infty} s(u)\cdot (g(u-t)\cdot e^{i\omega u})^* du \\ &= \int_{-\infty}^{+\infty} s(u)\cdot (g_\omega(u))^* du \\ &= \frac{1}{2\pi}\int_{-\infty}^{+\infty} \hat{s}(\xi)\cdot(\widehat{g_\omega}(\xi))^* d\xi \end{aligned} \tag{6}$$

where $()^*$ denotes complex conjugation, $\hat{s}(\xi)$ is the Fourier transform (FT) of $s(u)$, $\widehat{g_\omega}(\xi)$ is the FT of $g_\omega(u)$, and $g^* = g$ (the window g is real). Consider $\widehat{g_\omega}(\xi)$ to be calculated by

$$\widehat{g_\omega}(\xi) = \int_{-\infty}^{+\infty} g(u-t)\cdot e^{i\omega u}\cdot e^{-i\xi u}du. \tag{7}$$

Letting $u - t = t'$, we then have

$$\begin{aligned} &\widehat{g_\omega}(\xi) \\ &= \int_{-\infty}^{+\infty} g(t')\cdot e^{i\omega(t+t')}\cdot e^{-i\xi(t+t')}dt' \\ &= e^{i\omega t - i\xi t}\cdot \int_{-\infty}^{+\infty} g(t')\cdot e^{i\omega t' - i\xi t'}dt' \\ &= e^{i\omega t - i\xi t}\cdot \hat{g}(\omega-\xi) \end{aligned} \tag{8}$$

where $\hat{g}(\omega-\xi)$ is the FT of the window function. Then, substituting (8) into (6), we can obtain

$$\begin{aligned} &G(t,\omega) \\ &= \frac{1}{2\pi}\int_{-\infty}^{+\infty} \hat{s}(\xi)\cdot(e^{i\omega t - i\xi t}\cdot \hat{g}(\omega-\xi))^* d\xi \\ &= \frac{1}{2\pi}\int_{-\infty}^{+\infty} \hat{s}(\xi)\cdot e^{-i\omega t + i\xi t}\cdot \hat{g}(\omega-\xi) d\xi \\ &= e^{-i\omega t}\cdot\frac{1}{2\pi}\int_{-\infty}^{+\infty} \hat{s}(\xi)\cdot \hat{g}(\omega-\xi)\cdot e^{i\xi t} d\xi. \end{aligned} \tag{9}$$

When the regular STFT expression considers an additional phase shift $e^{i\omega t}$ as

$$G_e(t,\omega) = \int_{-\infty}^{+\infty} g(u-t)\cdot s(u)\cdot e^{-i\omega(u-t)}du. \tag{10}$$

Then the modified STFT (10) can be rewritten as

$$G_e(t,\omega) = \frac{1}{2\pi}\int_{-\infty}^{+\infty} \hat{g}(\omega-\xi)\cdot \hat{s}(\xi)\cdot e^{i\xi t}d\xi. \tag{11}$$

Herein, we employ the model of a purely harmonic signal (the frequency is ω_0) with invariant amplitude (A) as

$$s_h(t) = A\cdot e^{i\omega_0 t}. \tag{12}$$

Due to the FT of $s_h(t)$,

$$\hat{s}(\xi) = 2\pi A\cdot\delta(\xi-\omega_0). \tag{13}$$

Substituting (13) into (11), we can obtain the STFT of $s_h(t)$,

$$G_e(t,\omega) = A\cdot\hat{g}(\omega-\omega_0)\cdot e^{i\omega_0 t}. \tag{14}$$

According to (14), we have the following properties: (a) The STFT representation of the harmonic signal is constituted by a series of harmonic signals with the same frequency ω_0, which is consistent with the original signal $s_h(t)$. (b) Due to $|e^{i\omega_0 t}| = 1$ and $\hat{g}()$ being compact, the energy of the TF representation concentrates on the frequency $\omega = \omega_0$, and in this frequency region, the TF representation has the maximum amplitude, which is equal to $A\cdot\hat{g}(0)$.

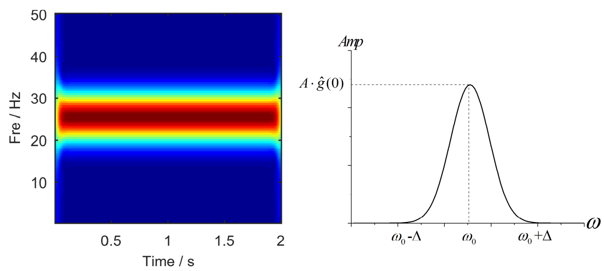

(a) (b)

Fig.1. (a) The spectrogram $|G_e(t,\omega)|$, (b) the spectrogram at t_0=1s, i.e. $|G_e(t_0,\omega)|$.

Herein, we employ a numerical signal ($s(t) = \cos(2\pi\cdot 25t)$, with a frequency of 25Hz and amplitude of 1) to conduct the above analysis and the following study. Fig. 1(a) shows the spectrogram. We can see that the TF energy is concentrated on ω_0=25Hz. Now, we take the slice of the spectrogram at $t_0 = 1s$, i.e., $|G_e(t_0,\omega)|$, as shown in Fig. 1(b), where Δ denotes the frequency support of the window function. It can be seen that the TF energy spreads in the region $[\omega_0-\Delta, \omega_0+\Delta]$

and reaches the maximum in the frequency ω_0. However, based on the energy-blurred result, it is impossible to characterize the time-varying feature of a signal precisely.

The SST method is designed to improve the energy concentration by a squeezing procedure. The relative theory is based on the usually-ignored IF information of the STFT. To obtain the IF of the STFT result (14), it is first suggested to calculate the derivative of $G_e(t,\omega)$ with respect to time as

$$\begin{aligned}&\partial_t G_e(t,\omega)\\&=\partial_t\left(A\cdot\hat{g}(\omega-\omega_0)\cdot e^{i\omega_0 t}\right)\\&=A\cdot\hat{g}(\omega-\omega_0)\cdot e^{i\omega_0 t}\cdot i\cdot\omega_0\\&=G_e(t,\omega)\cdot i\cdot\omega_0.\end{aligned}\tag{15}$$

The expression (15) leads to (16): for any (t,ω) and for which $G_e(t,\omega)\neq 0$, a two-dimensional IF $\omega_0(t,\omega)$ for the STFT result (14) can be obtained by

$$\omega_0(t,\omega)=-i\cdot\frac{\partial_t G_e(t,\omega)}{G_e(t,\omega)}.\tag{16}$$

The expression (16) illustrates one factor: in the two-dimensional TF plane, if $G_e(t,\omega)$ is not zero, the IF of the STFT coefficients should always be equal to ω_0. In Fig. 2(a), the IF $\omega_0(t,\omega)$ is displayed, and the $\omega_0(t,\omega)$ at the time $t_0=1s$ is listed as shown in Fig. 2(b). It can be seen that, in the TF region $\omega\in[\omega_0-\Delta,\ \omega_0+\Delta]$, the value is always equal to the signal frequency ω_0.

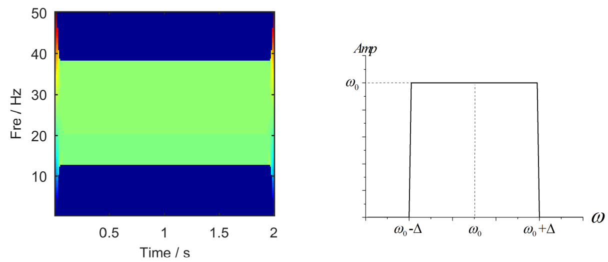

(a) (b)

Fig.2. (a) The IF $\omega_0(t,\omega)$, (b) the IF at t_0=1s, i.e. $\omega_0(t_0,\omega)$.

In the framework of SST, the IF $\omega_0(t,\omega)$ is used to gather the STFT coefficients that have the same frequency to where they should appear, which is called as synchrosqueezing. The gathering manner can be understood in Fig. 3(a) more clearly. In mathematics, the synchrosqueezing operator is written as $\int_{-\infty}^{+\infty}\delta(\eta-\omega_0(t,\omega))d\omega$, and the synchrosqueezing transform is formulated as

$$Ts(t,\eta)=\int_{-\infty}^{+\infty}G_e(t,\omega)\cdot\delta(\eta-\omega_0(t,\omega))d\omega.\tag{17}$$

By this post-processing procedure, we can obtain a sharper TF representation than the original STFT, as shown in Fig. 3(b). As a benefit of the reconstruction ability, the mono-component modes can be recovered from the SST result to a highly precise degree [6].

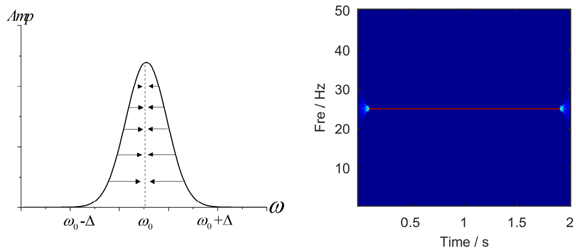

(a) (b)

Fig.3. (a) The gathering manner of operator $\int_{-\infty}^{+\infty}\delta(\eta-\omega_0(t,\omega))d\omega$, (b) the SST result $Ts(t,\eta)$.

In the framework of the SST method, all the TF coefficients from the original TF plane (t,ω) are squeezed into the IF region $\eta=\omega_0$ of a new TF plane (t,η). However, in practical cases, most signals contain noise, and the random noise may spread out over the entire TF plane. In the synchrosqueezing processing of TF coefficients, the unexpected noise has to be gathered into the SST result, which will result in bad noise robustness. According to (14), the original TF representation $|G_e(t,\omega)|$ can achieve the maximum value in the IF trajectory, and the TF coefficient $G_e(t,\omega_0)$ should have the best noise robustness. Thus, we are motivated to generate a novel TF representation only using the TF coefficient in the IF trajectory $\omega=\omega_0$ as in (18).

$$Te(t,\omega)=G_e(t,\omega)\cdot\delta(\omega-\omega_0(t,\omega)).\tag{18}$$

Observing (1) and (18), the proposed expression (18) can be regarded as using the amplitude and IF information of the STFT result to substitute the amplitude and IF of the ITFA, i.e., $G_e(t,\omega)\to A(t)$ and $\omega_0(t,\omega)\to\varphi'(t)$. Therefore, (18) is an effort to achieve the ITFA. According to the framework of the ITFA (1), in a TF plane, the signal energy of the ideal TF representation should only appear in $\omega=\varphi'(t)$. Reconsidering (18), the operator $\delta(\omega-\omega_0(t,\omega))$ can be interpreted as

$$\delta(\omega-\omega_0(t,\omega))=\begin{cases}1,\ \omega=\omega_0\\0,\ \omega\neq\omega_0\end{cases}.\tag{19}$$

Therefore, $\delta(\omega-\omega_0(t,\omega))$ can be regarded as a novel TF representation of binarization in the TF plane, as shown in Fig. 4.

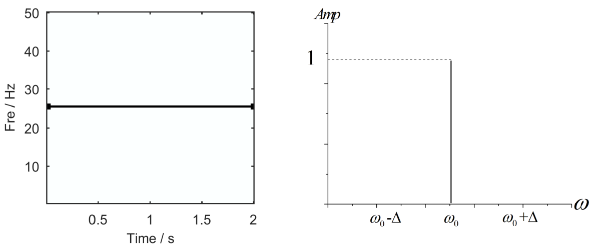

(a) (b)

Fig.4. (a) The operator $\delta(\omega-\omega_0(t,\omega))$, (b) the operator at t_0=1s, i.e. $\delta(\omega-\omega_0(t_0,\omega))$.

This article has been accepted for publication in a future issue of this journal, but has not been fully edited. Content may change prior to final publication. Citation information: DOI 10.1109/TIE.2017.2696503, IEEE Transactions on Industrial Electronics

From the above analysis, we see that the operator $\delta(\omega-\omega_0(t,\omega))$ can provide us with the following capability,

$$Te(t,\omega)=\begin{cases} G_e(t,\omega)\ , & \omega=\omega_0 \\ 0\ , & \omega\neq\omega_0 \end{cases}. \tag{20}$$

In theory, the operator $\delta(\omega-\omega_0(t,\omega))$ extracts the TF coefficient of $G_e(t,\omega)$ only in the IF trajectory $\omega=\omega_0$, and the rest of the TF coefficients are removed. This post-processing manner can be understood in Fig. 5(a) more clearly. It shows that most TF coefficients are removed and only the TF coefficient $G_e(t,\omega_0)$ is retained. By this extraction method, the novel TF representation $Te(t,\omega)$ (see Fig. 5(b)) can be more energy-concentrated than the original STFT result, and the TF resolution can be highly improved. Compared with the SST gathering all coefficients, the proposed method only utilizes the TF coefficient having maximum value to generate a novel TF representation, such that the effect of noises on the TF result can be minimized. Different from the squeezing manner of the SST method, the proposed method having extracting manner (18) is named the synchroextracting transform (SET) and $\delta(\omega-\omega_0(t,\omega))$ is called the synchroextracting operator (SEO).

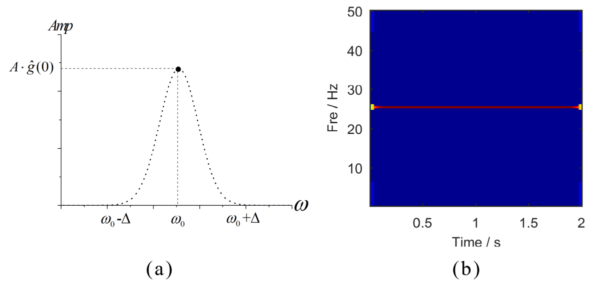

Fig. 5. (a) The extracting manner of operator $\delta(\omega-\omega_0(t,\omega))$ (the black solid point denotes the retained TF coefficient $G_e(t,\omega_0)$, and the dotted line denotes the removed TF coefficients). (b) the SET result $Te(t,\omega)$.

In discrete data processing, the partial derivative is commonly implemented approximately by a finite difference operator, i.e.

$$\partial_t G_e(t,\omega)\approx(G_e(t+\Delta t,\omega)-G_e(t,\omega))/\Delta t. \tag{21}$$

For more precise parameter estimation, $\partial_t G_e(t,\omega)$ can also be calculated by (22).

$$\begin{aligned} &\partial_t G_e(t,\omega) \\ &=\partial_t\left(\int_{-\infty}^{+\infty} g(u-t)\cdot s(u)\cdot e^{-i\omega(u-t)}du\right) \\ &=-\int_{-\infty}^{+\infty} g'(u-t)\cdot s(u)\cdot e^{-i\omega(u-t)}du \\ &+\ i\omega\cdot\int_{-\infty}^{+\infty} g(u-t)\cdot s(u)\cdot e^{-i\omega(u-t)}du \\ &=-G_e^{g'}(t,\omega)+i\omega\cdot G_e(t,\omega) \end{aligned} \tag{22}$$

where g' is the derivative of the window function with respect to time. Then, substituting (22) into (16), $\omega_0(t,\omega)$ can be obtained by (23).

$$\omega_0(t,\omega)=i\cdot\frac{G_e^{g'}(t,\omega)}{G_e(t,\omega)}+\omega. \tag{23}$$

Such that the SEO can be rewritten as (24).

$$SEO(t,\omega)=\delta(-i\cdot\frac{G_e^{g'}(t,\omega)}{G_e(t,\omega)}). \tag{24}$$

According to the Dirac function $\delta()$, the SEO should be calculated by (25).

$$SEO(t,\omega)=\begin{cases} 1, & -i\cdot\dfrac{G_e^{g'}(t,\omega)}{G_e(t,\omega)}=0 \\ 0, & -i\cdot\dfrac{G_e^{g'}(t,\omega)}{G_e(t,\omega)}\neq 0 \end{cases}. \tag{25}$$

However, considering the calculation error and that the SEO's real part needs to be utilized in practical applications [6], [17], it is suggested that (25) be rewritten as (26).

$$SEO(t,\omega)=\begin{cases} 1, & \left|\mathrm{Re}\left(i\cdot\dfrac{G_e^{g'}(t,\omega)}{G_e(t,\omega)}\right)\right|<\Delta\omega/2 \\ 0, & \left|\mathrm{Re}\left(i\cdot\dfrac{G_e^{g'}(t,\omega)}{G_e(t,\omega)}\right)\right|\geq\Delta\omega/2 \end{cases} \tag{26}$$

where $\Delta\omega=\omega_l-\omega_{l-1}$ is the discrete frequency interval and $\mathrm{Re}(\cdot)$ denotes taking the real part.

B. Multi-component signal processing and mode decomposition

In practice, it is often found that a measured signal is the superposition of several modes produced by distinct excitation sources. Each mode is an effective way to study the natural phenomena using their individually intrinsic behaviors. How to decompose a multi-component signal into the mono-component modes is another important application of the TFA method [18], [19]. For a signal such as (3), if the different modes are separated by sufficient distance, i.e.,

$$\varphi'_{k+1}(t)-\varphi'_k(t)>2\Delta \tag{27}$$

where $k\in\{1,...,n-1\}$, then each mono-component mode can be separated or reconstructed from the TF representation. With the assumptions that $\exists\varepsilon\ \varepsilon'$ small, $A'_k(t)\leq\varepsilon$ and $\varphi''_k(t)\leq\varepsilon'$ for $\forall t$, the STFT of signal (3) can be represented in the following first-order approximation form (28) [18], [20].

$$G_e(t,\omega)\approx\sum_{k=1}^{n}A_k(t)\cdot\hat{g}(\omega-\varphi'_k(t))\cdot e^{i\varphi_k(t)}. \tag{28}$$

For a well-separated multi-component signal, the expression (16) can also work for estimating the IF of each mode effectively [6], [17], which is calculated by

$$\varphi'(t,\omega)=\sum_{k=1}^{n}\varphi'_k(t,\omega)=-i\cdot\frac{\partial_t G_e(t,\omega)}{G_e(t,\omega)}. \tag{29}$$

In this case, the SET expression should be written as

$$Te(t,\omega)=G_e(t,\omega)\cdot\delta(\omega-\varphi'(t,\omega)). \tag{30}$$

A numerical signal consisting of several time-varying modes borrowed from [19] is analyzed, and the relative analysis results are shown in Fig. 6. In Fig. 6(a), each mode occupies

This article has been accepted for publication in a future issue of this journal, but has not been fully edited. Content may change prior to final publication. Citation information: DOI 10.1109/TIE.2017.2696503, IEEE Transactions on Industrial Electronics

distinct domains of the TF plane, and the corresponding energy spreads around their IF trajectories. Under the satisfaction of the separation condition (27), the estimated IF (see Fig. 6(b)) is equal to the superposition of individually estimated IFs of each mode. Furthermore, the SEO and SET results (see Fig. 6(c-d)) can be obtained just like dealing with the mono-component signal.

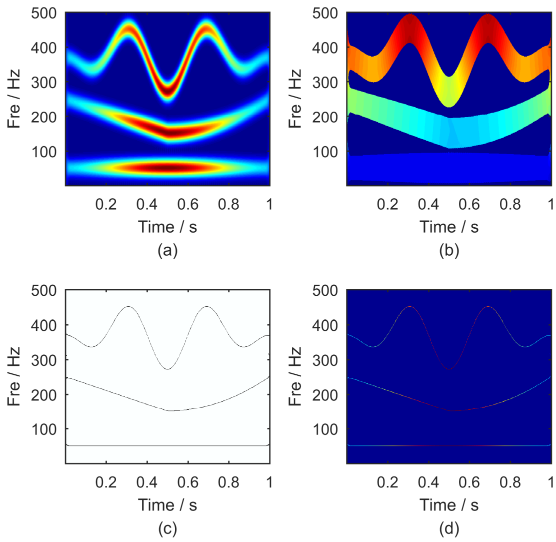

Fig.6. The relative analysis results of a numerical signal in [19], (a) the spectrogram $|G(t,\omega)|$, (b) the IF $\varphi'(t,\omega)$, (c)the SEO $\delta(\omega-\varphi'(t,\omega))$ and (d) the SET result $Te(t,\omega)$.

According to (28) and (30), we can deduce the following expression

$$\begin{aligned} Te(t,\omega)\big|_{\omega-\sum_{k=1}^{n}\varphi'_k(t)=0} &= G_e(t,\omega)\big|_{\omega-\sum_{k=1}^{n}\varphi'_k(t)=0} \\ &\approx \sum_{k=1}^{n} A_k(t)\cdot\hat{g}(0)\cdot e^{i\varphi_k(t)}. \end{aligned} \tag{31}$$

Therefore, signal (3) can be reconstructed approximately by

$$s(t) \approx \sum_{k=1}^{n} Te(t,\varphi'_k(t))/\hat{g}(0). \tag{32}$$

And each mode admits the following decomposition form (33) in a first-order approximation manner [18], [20].

$$s_k(t) \approx Te(t,\varphi'_k(t))/\hat{g}(0). \tag{33}$$

Herein, to compare the difference between the proposed SET and the SST, we also review the signal reconstruction or mode decomposition approach of the SST method. For the STFT (10), if we calculate the integral in the frequency direction, we can deduce the following expression (34):

$$\begin{aligned} &\int_{-\infty}^{+\infty} G_e(t,\omega)d\omega \\ &= \int_{-\infty}^{+\infty}\int_{-\infty}^{+\infty} g(u-t)\cdot s(u)\cdot e^{-i\omega(u-t)}du d\omega \\ &= 2\pi\cdot\int_{-\infty}^{+\infty} g(u-t)\cdot s(u)\cdot\delta(u-t)du \\ &= 2\pi g(0)\cdot s(t). \end{aligned} \tag{34}$$

Therefore, the original signal $s(t)$ can be reconstructed by

$$s(t) = (2\pi g(0))^{-1}\cdot\int_{-\infty}^{+\infty} G_e(t,\omega)d\omega. \tag{35}$$

According to (28), when the separation condition (27) is satisfied, different modes occupy their own TF domain without interference. To decompose each mode in the time domain, we can integrate the TF coefficients in only the frequency direction

$$s_k(t) = (2\pi g(0))^{-1}\cdot\int_{|\omega-\varphi'_k(t)|\le\Delta} G_e(t,\omega)d\omega. \tag{36}$$

Because the SST only considers the squeezing of TF coefficients in the frequency direction, that can be regarded as the integral calculation in the frequency direction, and the reconstruction expression of the SST is similar to that of STFT,

$$s_k(t) = (2\pi g(0))^{-1}\cdot\int_{|\omega-\varphi'_k(t)|\le ds} Ts(t,\omega)d\omega. \tag{37}$$

From (37), we know that, to reconstruct a mode, the SST integrates the TF coefficients around the IF of each mode. However, the integration region $\omega\in[\varphi'_k(t)-ds,\ \varphi'_k(t)+ds]$ is hard to determine in practice, and different integration regions may yield distinct reconstructed results [8]. According to the expression (33) and expression (37), to decompose a mono-component mode, both of SET and SST need to know the IF trajectories. However, apart from the parameter of IF trajectories, the SST has to know the integration regions additionally. Compared with SST, the SET reconstruction is more convenient and straight-forward.

III. Numerical Validation

To explore the performance of the proposed SET method comprehensively, we consider the following quantified indicators to illustrate its effectiveness, including the Rényi entropy of the TF representation, the ability of signal reconstruction and the required time for computation analysis. The comparison is made between various classical and advanced TFA methods, such as the STFT, SST, RS, PTFA and DTFA. To make the comparisons objective, we have written the code of all the above TFA methods in MATLAB, and the window function used in these methods is unified as a Gaussian window (38), since the Gaussian window function has the minimal area of the Heisenberg box.

$$g(t) = e^{-\pi\cdot t^2/0.32^2}. \tag{38}$$

In the processing of numerical signals and real-world signals, the comparisons are made between the proposed SET and the other TFA methods, such as the STFT, SST, RS, PTFA and DTFA. Because all the above-mentioned methods need to make use of a Gaussian window function, the window sizes applied in these Sections are listed in Table I. In discrete data processing, the time-shift of the window function $g(t)$ is one sampling interval, and therefore the window overlap should be equal to the window length minus the sampling interval.

TABLE I
THE WINDOW SIZES

TFA	Section III.A	Section III.B	Section IV.A	Section IV.B
STFT	0.4s	0.49s	0.315ms	0.025s
SST	0.4s	0. 49s	0.315ms	0.025s
RS	0.4s	0. 49s	0.315ms	0.025s
SET	0.4s	0. 49s	0.315ms	0.025s
PTFA	1.5s	2.92s	1.05ms	0.09s
DTFA	1.5s	2.92s	1.05ms	0.09s

This article has been accepted for publication in a future issue of this journal, but has not been fully edited. Content may change prior to final publication. Citation information: DOI 10.1109/TIE.2017.2696503, IEEE Transactions on Industrial Electronics

A. A mono-component signal

A frequency-modulated (FM) and amplitude-modulated (AM) signal is selected first to illustrate the comparison, and it is modeled as

$$s(t) = e^{-0.5 \cdot t} \cdot \sin(2\pi \cdot (25 \cdot t + 10 \cdot \sin(1.5 \cdot t))) \tag{39}$$

whose sampling frequency is 100Hz and sampling time is 4s. According to signal expression (39), the IF and IA trajectories are drawn in Fig. 7(a-b), and the corresponding ITFA representation is generated in Fig. 7(c-d). The ITFA representation demonstrates the fact that, in each time interval, only one frequency bin appears to describe this mono-component signal in the TF plane.

The TF representation in Fig. 8(a) results from the STFT, which suffers from a poor TF resolution. In Fig. 8(b), the SEO is displayed. It can be seen that, the SEO is a TF representation that is independent of the signal amplitude, and it is a good approximation of the signal IF. Utilizing the STFT result and SEO result, we can obtain the SET representation (see Fig. 8(c-d)), which shows an obviously higher energy concentration than the STFT.

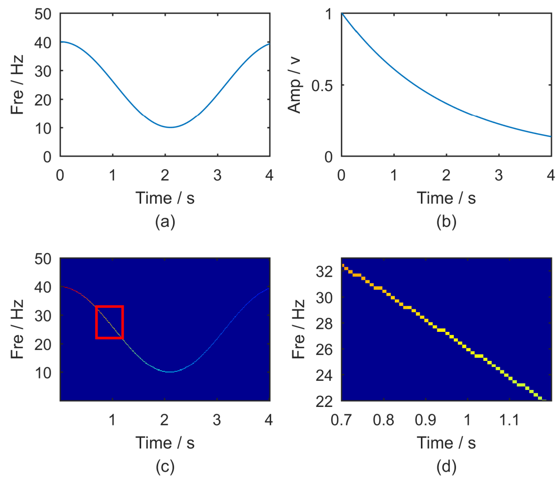

Fig. 7. (a) The IF trajectory, (b) the IA trajectory, (c) the ITFA representation and (d) the corresponding zoom of the ITFA.

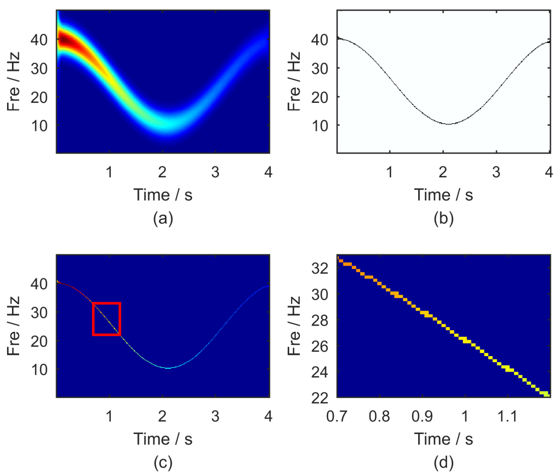

Fig. 8. (a) STFT result, (b) SEO, (c) SET result and (d) zoom of the SET result.

For comparison, we list the TF representation generated by the SST, RS, (see Fig. 9) PTFA and DTFA methods (see Fig. 10). Both provide more energy-concentrated TF results than the STFT. In 0.8 s ~ 1.2 s, the signal has a rapidly decreasing FM law. As shown in the zoom of the SST result, it is blurry, since the SST squeezes the TF coefficients only in the frequency direction. However, the RS reassigns the TF spectrogram in the two-dimensional TF direction such that the corresponding TF result is more concentrated.

The PTFA and DTFA methods are iterative algorithms, and the TF results are generated step by step. Herein, we only list the TF results of the last step, as shown in Fig. 10, where the polynomial model is selected as the parameter input. The superiority of the PTFA and DTFA methods comes from the use of the non-linear TF basis function, such that the generated results are more concentrated than the STFT result. However, the use of the inner product must be restricted by the Heisenberg uncertainty principle, such that the best time resolution and frequency resolution cannot be simultaneously achieved.

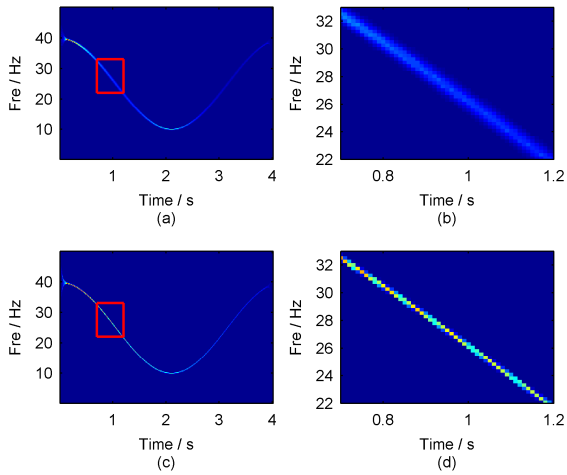

Fig. 9. (a) SST result, (b) zoom of the SST result (c) RS result and (d) zoom of the RS result.

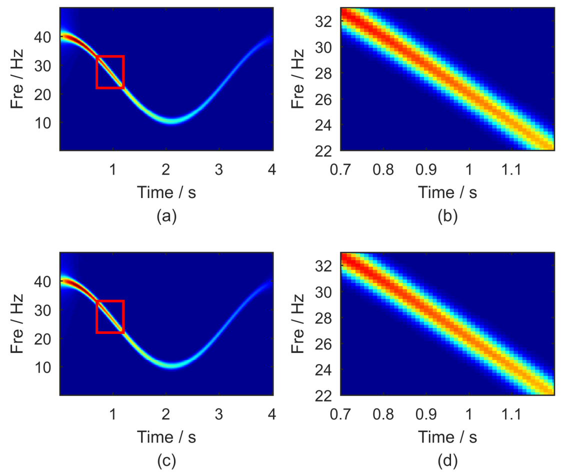

Fig. 10. (a) PTFA result, (b) zoom of the PTFA result (c) DTFA result and (d) zoom of the DTFA result.

The more energy-concentrated TF result denotes the better ability of the TF location and the better characterization of the time-varying feature. The Rényi entropy is an objective indicator to evaluate the energy concentration of a TF result. Therefore, the Rényi entropy is employed to evaluate the performance of different methods quantitatively, and a lower Rényi entropy value denotes a more energy-concentrated TF representation. The corresponding Rényi entropies are listed in Table II. It can be seen that, the SET result has the lowest Rényi entropy, which denotes that it can generate the most energy-concentrated TF representation. Just from the visual representation, the SET result is the closest to the ITFA representation among all the TFA methods.

TABLE II
RÉNYI ENTROPY

TFA	STFT	PTFA	DTFA	SST	RS	SET
Rényi Entropy	13.5859	11.9333	11.9510	9.6191	8.8601	8.3261

Both the SET and SST allow for signal reconstruction, so it is necessary to test the ability of signal recovery under different level noises. The white noises with SNRs (signal to noise ratio) of 1 dB to 30 dB are added to the signal (39). For the SET reconstruction expression (33), to recover a signal, it needs one parameter $\varphi'_k(t)$, i.e., the IF trajectory corresponding to each mode. For the mono-component signal, the IF trajectory can be estimated by the maximum value detection method directly, i.e., $\varphi'(t)=\arg\max_{\omega}|TFR(t,\omega)|$, where $TFR(t,\omega)$ denotes the TF representation to be analyzed. For the SST reconstruction expression (37), apart from the parameter $\varphi'_k(t)$, it needs to know the integration parameter ds. For the strong FM signal, the SST result smears heavily [21]. To recover the original signal, a more smeared TF representation means that more TF coefficients are needed. Therefore, the parameter ds cannot be given a certain value. Herein, we consider three different integration parameters, ds=5,10,15 . The SNRs of the reconstructed results are calculated and listed in Fig. 11. It can be found that, for the SST reconstruction, more TF coefficients (ds=15) yield more noise-robust results. In the low SNR case (1-15 dB), the SET has similar performance to that of the SST with ds=15. In the high SNR case (16-30 dB), restricted to the first-order approximation method, the SET cannot provide more accurate reconstruction results. Compared to the SST, because the SET reconstruction just needs to know the parameter $\varphi'_k(t)$, it is more straight-forward and convenient.

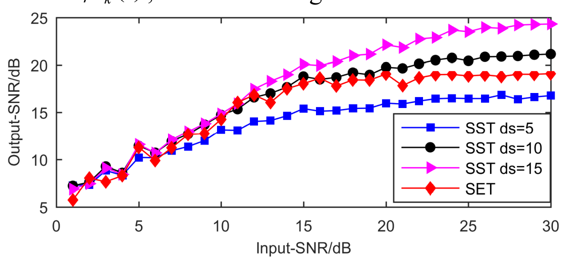

Fig. 11. Under different noise levels (SNRs of 1 dB-30 dB), the SNR of the reconstructed results by different TFA methods.

The efficiency of a TFA method is important in real-time applications and decides whether or not the method can be used in practical engineering. Herein, we test the computational time required for the above-mentioned TFA methods, generating the TF representations in Figs. 8–10. The tested computer configuration is as follows: Intel Core i7-6500 2.5 GHz, 8.0 GB of DDR3 RAM, Windows 10 OS, and MATLAB version R2016a. The computation times required are listed in Table III. It can be seen that, the computational burden of the SET method is approximately twice that of the STFT method. That is because the SET method needs to calculate $G_e(t,\omega)$ and $G_e^{g'}(t,\omega)$ at the same time.

TABLE III
REQUIRED COMPUTATION TIME

TFA	STFT	PTFA	DTFA	SST	RS	SET
Time(s)	0.028	0.066	0.059	0.070	0.062	0.053

B. A multi-component signal

In this section, we consider a multi-component signal consisting of three modes. The sampling frequency is 120 Hz, and the sampling time is 4 s. The math model is written as

$$\begin{aligned} s_1(t) &= \sin(2\pi\cdot(44\cdot t+10\cdot\sin(t))) \\ s_2(t) &= \sin(2\pi\cdot(32\cdot t+10\cdot\sin(t))) \\ s_3(t) &= \sin(2\pi\cdot(10\cdot t+2\cdot\arctan((2\cdot t-2)^2))). \end{aligned} \tag{40}$$

The corresponding IF trajectory and ITFA representation are drawn in Fig. 12. It can be seen that the modes $s_1(t)$ and $s_2(t)$ have the same FM law but distinct initial frequencies, and the mode $s_3(t)$ has an arc-tangent trend FM law.

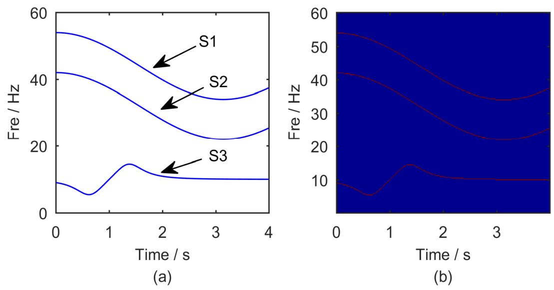

Fig. 12. (a) The IF trajectories and (b) the ITFA representation.

To test the noise robustness of the proposed method, the signal (40) has the white noise added to it (the SNR is from 1 dB to 30 dB). First, we focus on the Rényi entropies of the TF representations generated by different methods (see Fig. 13). It can be found that the increased noises enlarge the Rényi entropies, which means that the noise can deduce the energy concentration of these methods. The DTFA and PTFA methods provide almost the same results, which are less than the STFT but more than the SST and RS methods. Furthermore, it can be seen that, among all TFA methods, the SET results achieve the minimum in each noise level, which denotes that the SET has the best ability to improve the TF energy concentration.

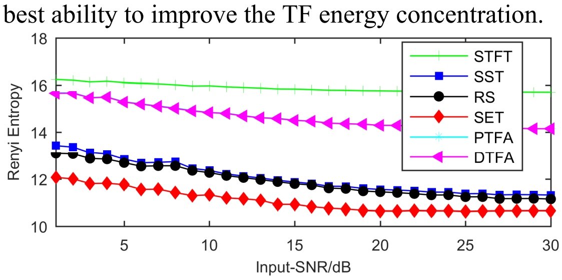

Fig. 13. Under different noise levels (SNR of 1 dB-30 dB), the Rényi entropies of the TF representations generated by different TFA methods.

This article has been accepted for publication in a future issue of this journal, but has not been fully edited. Content may change prior to final publication. Citation information: DOI 10.1109/TIE.2017.2696503, IEEE Transactions on Industrial Electronics

Moreover, to explore the differences of the above TFA methods in dealing with multi-component signals, we list the corresponding TF representations in Fig. 14 (the signal's SNR is equal to 6 dB). The time-varying feature in the STFT result (see Fig. 14(a)) is heavily affected by noises. Benefitting from the post-operation on the STFT representation, we can obtain the SST, RS and SET results (see Fig. 14(b-d)), whose TF energy concentration is enhanced greatly.

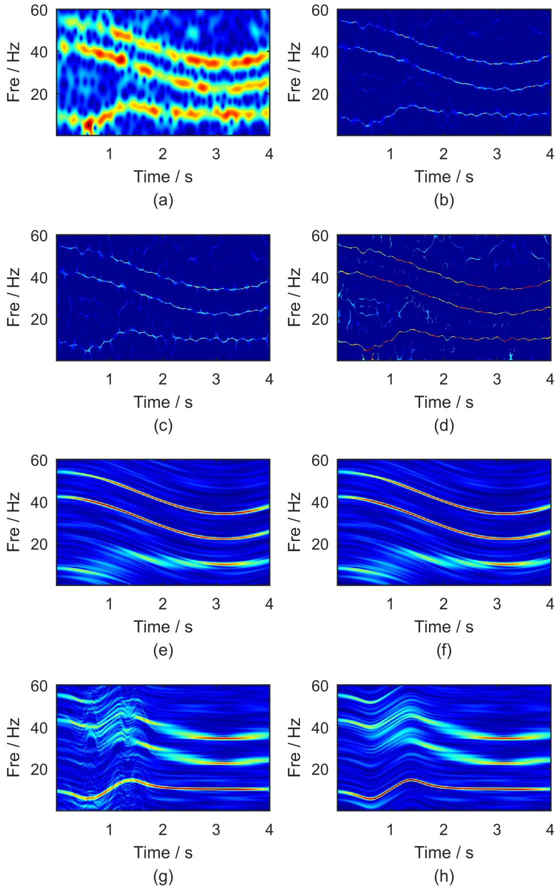

Fig. 14. (a) STFT result, (b) SST result, (c) RS result, (d) SET result, (e) PTFA result and (f) DTFA result by demodulating mode $s_1(t)$, (g) PTFA result and (h) DTFA result by demodulating mode $s_3(t)$.

For the PTFA and DTFA methods, before dealing with the signal, it is necessary to select the appropriate parameter to demodulate the time-varying component based on a *priori*. First, the mode $s_1(t)$ with the polynomial FM law is considered as the component that is to be demodulated. Compared with the STFT result, although the PTFA and DTFA results (see Fig. 14(e-f)) can provide better energy concentration for mode $s_1(t)$, the TF feature of mode $s_3(t)$ almost disappears. That is because the selected parameter can only demodulate the specified component and that with the same time-varying law, such as mode $s_2(t)$. However, the TF feature of mode $s_3(t)$ with the distinct FM trend is even worse than that of the STFT result. Then, to make a comparison, mode $s_3(t)$ is considered as the component to be demodulated, and the processing results are shown in Fig. 14(g-h). It can be observed that mode $s_3(t)$ is characterized clearly, but the TF features of modes $s_1(t)$ and $s_2(t)$ show poor energy concentration. Herein, we can conclude that the PTFA and DTFA methods are not suitable for processing the signal consisting of multiple components with distinct FM laws simultaneously.

Regardless of whether it is for the SST or for the SET, to decompose the mono-component modes in a multi-component signal, the first step is to estimate the IF trajectories corresponding to each mode. However, the maximum value detection method only works for mono-component signals. To estimate all IF trajectories at the same time, a popular multi-ridge detection algorithm is employed [18], [20], [22]. Knowing the number K of modes, this algorithm calculates the local minimum value of the function (41).

$$\begin{aligned} E(\phi) = \sum_{k=1}^{K} -\int_{-\infty}^{+\infty} \left|TFR(t,\phi_k(t))\right|^2 dt \\ +\int_{-\infty}^{+\infty} \left(\lambda \cdot \phi'_k(t)^2 + \beta \cdot \phi_k(t)^2\right) dt. \end{aligned} \tag{41}$$

where $\sum_{k=1}^{K}(t,\phi_k(t))$ is the estimation of the IF trajectories in the TF plane, and λ β are two parameters to adjust the level of regularization. The signal (40) with different levels of noises (SNR=20 dB, SNR=3 dB) is analyzed, and the parameter are set as K=3. The SST and SET results and the estimated IF trajectories are displayed in Fig. 15 and Fig. 16, respectively. It can be observed that, for the high SNR level (see Fig. 15), both the SST and SET can provide clear TF representations to be analyzed, and the IF trajectories are estimated correctly. However, for the low SNR level (see Fig. 16(a)), the energy of the SST result smears heavily, and the time-varying features of the three modes are blurry visually. In Fig. 16(b), the estimated IF trajectories based on the SST result even overlap with each other. In Fig. 16(c-d), although the SET result is affected by noises, the IF trajectories corresponding to the three modes are still well-estimated. It can be concluded that, in the aspect of IF estimation, the SET result has better noise-robustness than the SST result.

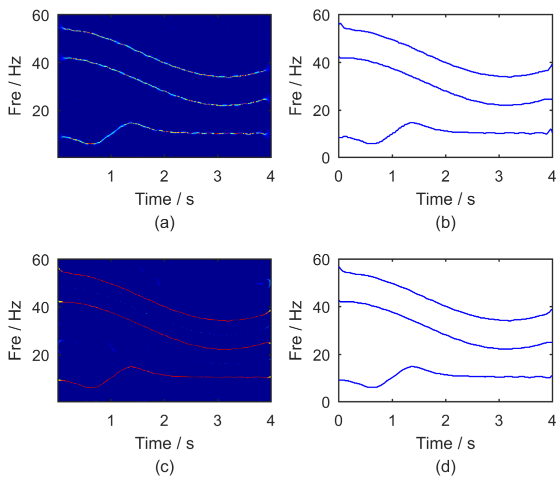

Fig. 15. The SNR added to the signal is equal to 20dB, (a) SST result, (b) the estimated IF trajectories, (c) SET result and (d) the estimated IF trajectories.

This article has been accepted for publication in a future issue of this journal, but has not been fully edited. Content may change prior to final publication. Citation information: DOI 10.1109/TIE.2017.2696503, IEEE Transactions on Industrial Electronics

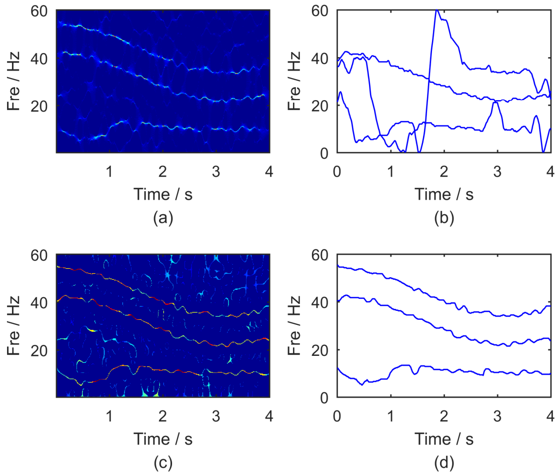

Fig. 16. The SNR added to the signal is equal to 3dB, (a) SST result, (b) the estimated IF trajectories, (c) SET result and (d) the estimated IF trajectories.

Benefitting from the estimated IF trajectories, the three mono-component modes can be reconstructed. The reconstruction performance is evaluated by the SNR of the superposition of the three decomposed modes. Under the different level noises, the reconstruction results are shown in Fig. 17. For 1-5 dB, the SET has the best reconstruction performance since the IF trajectories can be estimated from the SET result more accurately than the SST result, especially in the low SNR case. For 6-20 dB, the SET and SST provide similar reconstruction results. For the much higher SNR case (21-30 dB), the SST (ds=10,15) can achieve much better signal reconstruction than the SET because the SET reconstruction is mainly restricted to the first-order approximation method in the high SNR case. Herein, we can conclude that, in the low SNR case, with the aid of better performance on IF estimation, the SET reconstruction is more robust to noise than the SST.

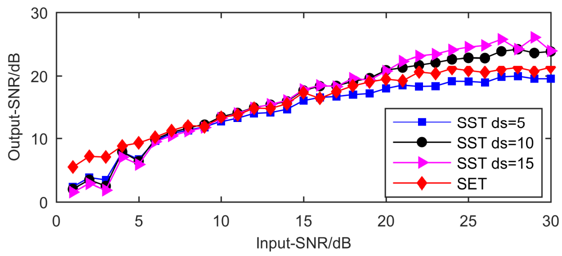

Fig. 17. Under different noise levels (SNR of 1 dB-30 dB), the SNR of the reconstructed results by different TFA methods.

IV. Experimental Validation

The SET is designed to analyze the AM-FM signal to help us understand this non-stationary world more clearly. In this section, we use two real-world signals to show the effectiveness of our proposed method.

A. *Bat Signal*

A popular bat signal recorded by Rice University is employed to be the first case to validate the proposed method [8], [19]. By producing the frequency-modulated and sweeping-downward signal, and collecting the echo-delay signal, the bats can identify the object successfully in the complex environment. This signal is sampled at 400 points and its sampling frequency is 140kHz. In Fig. 18, the waveform and the spectrum are displayed. However, just from the information in Fig. 18, it is hard to understand the non-linear behaviors of bat echolocation precisely.

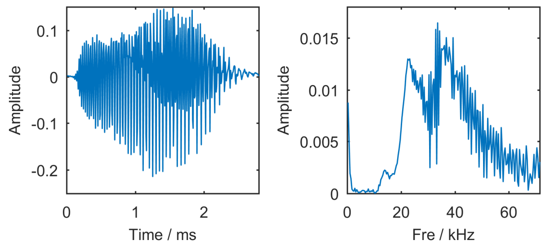

Fig. 18. The waveform of the bat signal and its spectrum.

Compared with the one-dimensional analysis in the time domain or frequency domain, with the aid of TFA technology, the time-varying features can be expanded into the two-dimensional TF plane to provide more essential information. By the processing of the STFT, a TF representation is shown in Fig. 19(a). Although the energy of the STFT result smears heavily, the basic FM-AM features can be characterized generally. By means of improving the energy concentration, the SET method is proposed to acquire better TF location ability. In Fig. 19(b), the SEO representation shows the FM laws of all modes contained in the bat signal. Because the SEO result is independent of the signal amplitude, it is very helpful to determine the number of all modes and discover the amplitude-weak components. In Fig. 19(c-d), both the FM law and AM trend are contained in the SET result. The zoom on the SET result provides a visual comparison with other TFA methods through observation. Compared with the STFT, the SET provides an obviously sparser representation to describe this bat signal.

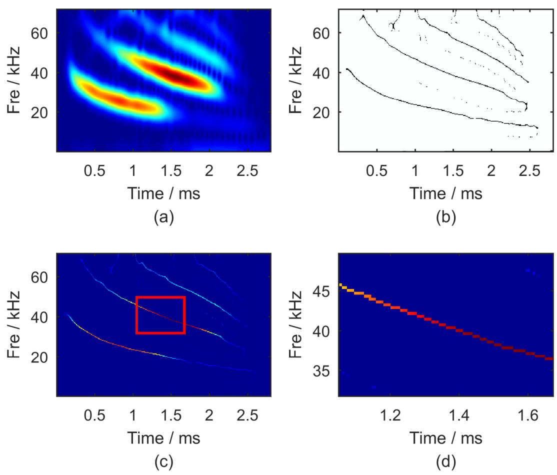

Fig. 19. (a) STFT result, (b) SEO, (c) SET result and (d) zoom of the SET result.

For furthermore comparison, the analyzed results generated by the SST, RS, PTFA and DTFA methods are shown in Fig. 20 and Fig. 21. The corresponding Rényi entropies are listed in Table IV. No matter from quantified Rényi entropies or through observation, the analysis results show that the SET has the best ability to generate the most energy-concentrated TF representation among all TFA methods.

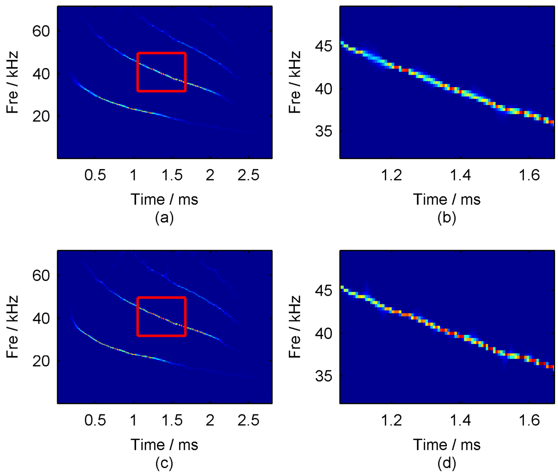

Fig. 20. (a) SST result, (b) zoom of SST result, (c) RS result and (d) zoom of RS result.

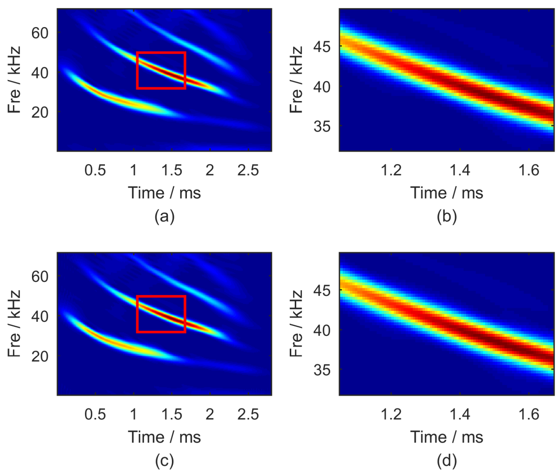

Fig. 21. (a) PTFA result, (b) zoom of the PTFA result, (c) DTFA result and (d) zoom of the DTFA result.

TABLE IV
RÉNYI ENTROPY

TFA	STFT	PTFA	DTFA	SST	RS	SET
Rényi Entropy	14.5456	13.3865	13.3511	10.1796	9.9599	9.4684

To make sure that all mono-component modes can be well-decomposed, it is first necessary to know the number of modes in the signal. In Fig. 19(b), it can be observed that four FM trajectories are characterized, which should correspond to four modes. Therefore, for algorithm (41), the parameter are set as $K=4$. Based on the SET, SST, RS and DTFA results, the estimated IF trajectories are plotted in Fig. 22. It can be seen that the estimation based on the SET result gives the best description of the IF trajectories. In Fig. 22(b-c), the estimated IF trajectories based on the SST and RS results overlap with each other partially. The DTFA result fails to provide useful information regarding the FM laws. In the processing of this bat signal, regardless of whether it improves the energy concentration or detects time-varying features, the proposed SET method has the best performance among the above-mentioned TFA methods.

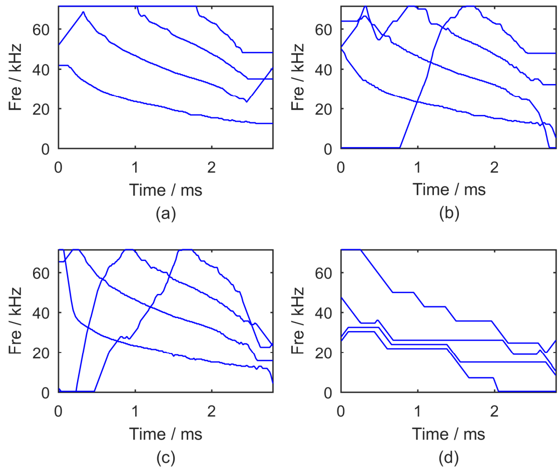

Fig. 22. The estimated IF trajectories based on (a) the SET result, (b) SST result, (c) RS result and (d) DTFA result.

Utilizing the IF trajectories estimated by the SET result, the mono-component modes can be decomposed effectively. The four decomposed modes are shown in Fig. 23. In Fig. 23(e), we list the summation of four components and the original bat signal (the black solid line is the original signal and the red dotted line is the summation of the four decomposed components). Their errors are plotted in Fig. 23(f). It can be seen that, the reconstruction errors are small compared to the original signal, which denotes that the proposed method has good invertible ability.

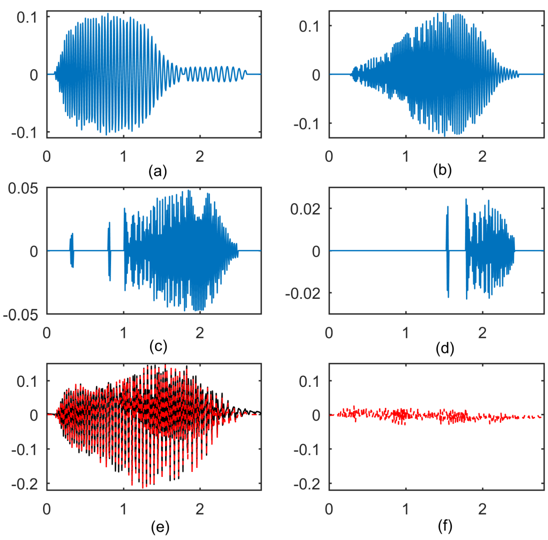

Fig. 23. (a-d) Four decomposed mono-component modes, (e) summation of the four modes (red) and the original signal (black), (f) reconstruction errors between the summation and the original signal.

B. Fault Vibration Signal

In this section, we focus on an abnormal vibration of a heavy oil catalytic machine set [13], whose structural sketch is shown in Fig. 24. It consists of a gas turbine, compressor, gearbox, and motor. The bearing cases (1#, 2#, 3# and 4#) are used to support

This article has been accepted for publication in a future issue of this journal, but has not been fully edited. Content may change prior to final publication. Citation information: DOI 10.1109/TIE.2017.2696503, IEEE Transactions on Industrial Electronics

the corresponding shaft. The rotation speed of the gas turbo is 5381 rpm (approximately 90 Hz). The vibration sensors are mounted on the bearing cases with a sampling frequency of 2 kHz.

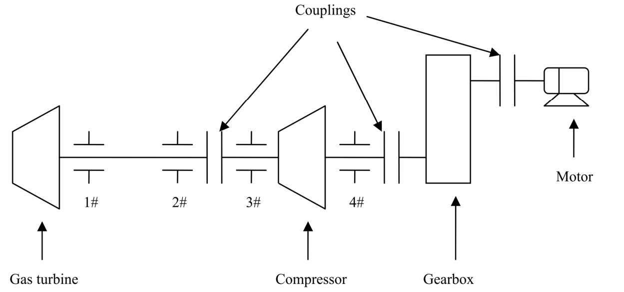

Fig. 24. A structural sketch of the machine set.

In the running state, the vibration in bearing 2# is larger than the alarm limitation. Thus, we take the signal recorded in bearing 2# for analysis. The vibration signal and its spectrum are shown in Fig. 25. It can be seen that the vibration signal consists of the first order (1X) component of the rotation frequency and its higher-order components. The 1X component has the largest energy, which should be the main cause of the abnormal vibration.

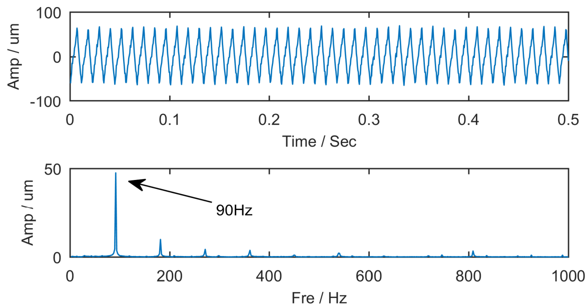

Fig. 25. The waveform of the vibration signal and its spectrum.

It is known that the IF of the 1X component corresponds to the instantaneous speed of the gas turbine shaft, which can reflect the current rotation condition. Therefore, we list the TF results in the frequency bank of 60 Hz-120 Hz created by different TFA methods. The STFT result (see Fig. 26(a)) is a coarse spectrum line that cannot provide accurate time-varying information. The TF results generated by the SST, RS and SET show some periodic oscillatory behaviors, as shown in Fig. 26(b-d). Visually, the energy of the SST and RS results smears heavily, while the SET result obviously looks more energy-concentrated.

Considering that the vibration signal has an oscillatory frequency, for the PTFA and DTFA method, we select the Fourier model as the parameter input. In Fig. 26(e-f), the PTFA and DTFA results are listed. It can be seen that, although the oscillatory features are characterized, the TF energy of both TF results obviously smears more heavily than that of the SET result.

By detecting the peak data of the SET result, we redraw the oscillatory IF of the 1X component in Fig. 27 and calculate its spectrum, which shows the same frequency with the rotation frequency. If a rub-impact fault exists between the rotor and the static element, then during each rotation, it will cause the local speed-down and speed-up effect on the shaft. The oscillatory frequency of the instantaneous speed should be equal to the rotating frequency. Therefore, this oscillatory phenomenon of bearing 2# points to the existence of a rub-impact fault.

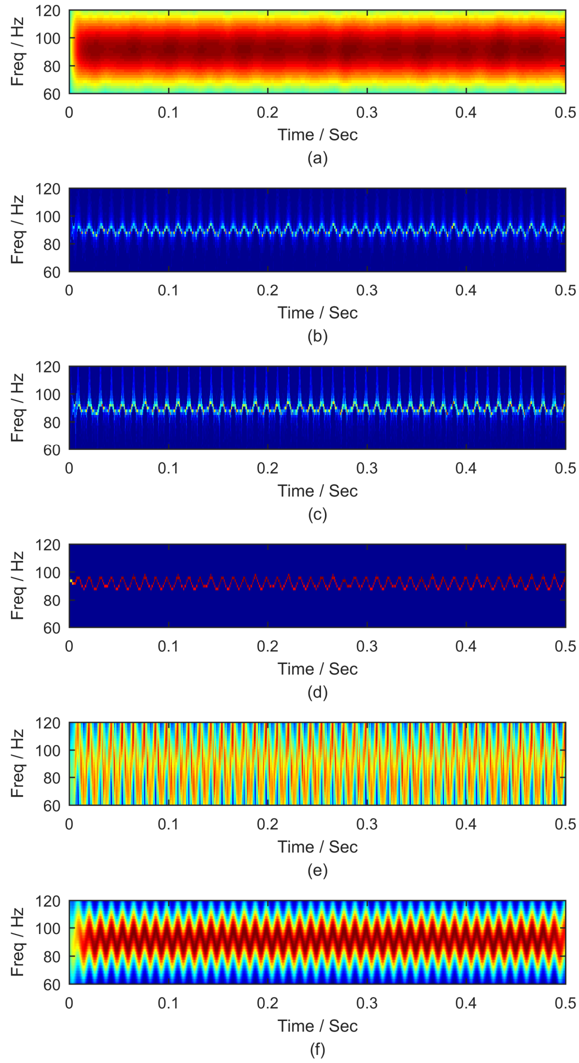

Fig. 26. (a) STFT result, (b) SST result, (c) RS result, (d) SET result, (e) PTFA result and (f) DTFA result.

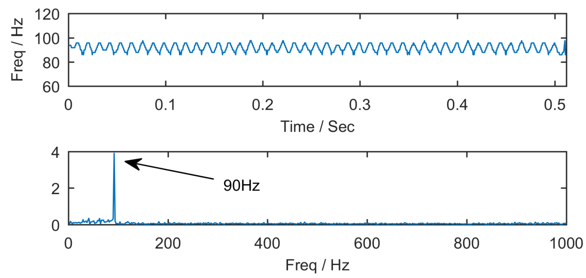

Fig. 27. The IF trajectory of the 1X component of the SET result and its spectrum.

V. CONCLUSION

Because the TF basis function used in linear TFA methods is bandwidth-wide in the time-frequency domain, the TF representation resulting from the inner product transform with the TF basis must be restricted by the Heisenberg uncertainty principle, such that the energy of the generated TF representation smears heavily. In this paper, we propose a novel TFA method, called the SET, whose purpose is to improve the energy concentration of the TF representation. Via a post-processing method, the most-smeared TF energy is removed, and only the TF information related to signal time-varying features is retained. Simultaneously, the novel TF result allows for signal reconstruction and mode decomposition. In the processing of numerical signals and real-world signals, we focus on the comparison of the SET method with other classical and advanced TFA methods. By comparison, it can be concluded that, our proposed method has the best performance in improving the energy concentration. In the low SNR case, the SET method can provide better estimation of IF trajectories than the SST method, such that the reconstructed signals based on the SET result are more robust to noise than that based on the SST result. In the high SNR case, although the SET cannot give more accurately reconstructed results than the SST (ds=15), the reconstruction method of the SET is more convenient and straight-forward than that of the SST, because the SET needs fewer parameters to reconstruct a signal.

In this study, the SET is discussed as a post-processing tool for the STFT. In theory, this post-processing method can also be grafted into other TFA methods, such as the wavelet transform, S transform, and even PTFA and DTFA methods.

A MATLAB implementation of the proposed algorithm is available at: http://cn.mathworks.com/matlabcentral/fileexchange/62483.

REFERENCES

[1] J. Pons-Llinares, J. A. Antonino-Daviu, M. Riera-Guasp, S. B. Lee, T.-j. Kang, and C. Yang, “Advanced induction motor rotor fault diagnosis via continuous and discrete time–frequency tools,” IEEE Trans. Ind. Electron., vol. 62, no. 3, pp. 1791-1802, Mar. 2015.

[2] F. Vedreno-Santos, M. Riera-Guasp, H. Henao, M. Pineda-Sanchez, and R. Puche-Panadero, “Diagnosis of rotor and stator asymmetries in wound-rotor induction machines under nonstationary operation through the instantaneous frequency,” IEEE Trans. Ind. Electron., vol. 61, no. 9, pp. 4947-4959, Sep. 2014.

[3] S. Qian and D. Chen, “Joint time–frequency analysis,” IEEE Signal Process. Mag., vol. 16, no. 2, pp. 52–67, Mar. 1999.

[4] F. Auger and P. Flandrin, “Improving the readability of time-frequency and time-scale representations by the reassignment method,” IEEE Trans. Signal Process., vol. 43, no. 5, pp. 1068–1089, May 1995.

[5] F. Auger, P. Flandrin, Y. Lin, S. McLaughlin, S. Meignen, T. Oberlin,and H. Wu, “Time-frequency reassignment and synchrosqueezing: Anoverview,” IEEE Signal Process. Mag., vol. 30, no. 6, pp. 32–41, Nov. 2013.

[6] I. Daubechies, J. Lu, and H.-T. Wu, “Synchrosqueezed wavelet transforms: An empirical mode decomposition-like tool,” Appl. Comput. Harmon. Anal., vol. 30, no. 2, pp. 243–261, Mar. 2011.

[7] S. Wang et al., “Matching demodulation transform and synchrosqueezing in time-frequency analysis,” IEEE Trans. Signal Process., vol. 62, no. 1, pp. 69–84, Jan. 2014.

[8] T. Oberlin, S. Meignen, and V. Perrier, “Second-order synchrosqueezing transform or invertible reassignment? Towards ideal time-frequency representations,” IEEE Trans. Signal Process., vol. 63, no. 5, pp. 1335–1344, Mar. 2015.

[9] Z. K. Peng, G. Meng, F. L. Chu, Z. Q. Lang, W. M. Zhang, andY. Yang, “Polynomial chirplet transform with application to instantaneous frequency estimation,” IEEE Trans. Instrum. Meas., vol. 60, no. 9, pp. 1378–1384, Sep. 2011.

[10] Y. Yang, W. Zhang, Z. Peng, and G. Meng, “Multicomponent signal analysis based on polynomial chirplet transform,” IEEE Trans. Ind. Electron., vol. 60, no. 9, pp. 3948–3956, Sep. 2013.

[11] Y. Yang, Z. K. Peng, G. Meng, and W. M. Zhang, “Spline-kernelled Chirplet transform for the analysis of signals with time-varying frequency and its application,” IEEE Trans. Ind. Electron., vol. 59, no. 3, pp. 1612-1621, Mar. 2012.

[12] W. Yang, P. J. Tavner, and W. Tian, “Wind Turbine Condition Monitoring Based on an Improved Spline-Kernelled Chirplet Transform,” IEEE Trans. Ind. Electron., vol. 62, no. 10, pp. 6565-6574, Oct. 2015.

[13] S. Wang, X. Chen, G. Li, X. Li, and Z. He, “Matching demodulation transform with application to feature extraction of rotor rub-impact fault,” IEEE Trans. Instrum. Meas., vol. 63, no. 5, pp. 1372–1383, May 2014.

[14] LJ. Stanković, I. Djurović, S. Stanković, M. Simeunović, S. Djukanović, and M. Daković, “Instantaneous frequency in time-frequency analysis: Enhanced concepts and performance of estimation algorithms,” Digit. Signal Process., vol. 35, pp. 1–13, Dec. 2014.

[15] N. E. Huang, Z. Shen, S. R. Long, M. C. Wu, H. H. Shih, Q. Zheng, N. C. Yen, C. C. Tung, and H. H. Liu, “The empirical mode decomposition and the Hilbert spectrum for nonlinear and non-stationary time series analysis,” Proc. R. Soc. London A, vol. 454, no. 1971, pp. 903–995, Mar. 1998.

[16] J. A. Rosero, L. Romeral, J. A. Ortega, and E. Rosero, “Short-circuit detection by means of empirical mode decomposition and Wigner–Ville distribution for PMSM running under dynamic condition,” IEEE Trans. Ind. Electron., vol. 56, no. 11, pp. 4534-4547, Nov. 2009.

[17] G. Thakur and H.-T. Wu, “Synchrosqueezing-based recovery of instantaneous frequency from nonuniform samples,” SIAM J. Math. Anal., vol. 43, no. 5, pp. 2078–2095, Sep. 2011.

[18] Meignen S, Oberlin T, Depalle P, Flandrin P, McLaughlin S. “Adaptive multimode signal reconstruction from time–frequency representations,” Phil. Trans. R. Soc. A, vol. 374, no. 2065, Apr. 2016.

[19] Wang S, Chen X, Tong C, et al. “Matching Synchrosqueezing Wavelet Transform and Application to Aeroengine Vibration Monitoring,” IEEE Trans. Instrum. Meas., vol. 66, no. 2, pp. 360–372, Jan. 2017.

[20] R. Carmona, W. Hwang, and B. Torrésani, “Multiridge detection and time-frequency reconstruction,” IEEE Trans. Signal Process., vol. 47, no. 2, pp. 480–492, Feb. 1999.

[21] D. Iatsenko, P. V. E. McClintock, and A. Stefanovska, "Linear and synchrosqueezed time-frequency representations revisited: Overview, standards of use, resolution, reconstruction, concentration, and algorithms," Digital Signal Process., vol. 42, pp. 1–26, Jul. 2015.

[22] Pham D H, Meignen S. High-order synchrosqueezing transform for multicomponent signals analysis-with an application to gravitational-wave signal. IEEE Trans. on Signal Process., Doi: 10.1109/TSP.2017.2686355, in press, 2017.

Gang Yu received the B.Eng. degree in mechanical engineering from Qingdao University, Qingdao, China, in 2010 and the Ph.D. degree in Mechanical Engineering from Shandong University, Jinan, P. R. China, in 2016.

He is currently a Lecturer of Mechanical Engineering with Jinan University. His current research interests include time-frequency analysis, blind source separation, modal identification and machinery condition monitoring and fault diagnosis.

Mingjin Yu received the M.S. degree in Power Mechanical Engineering from Shandong University. He is currently a professor of Vehicle Engineering in Shandong Jiaotong University. His current research interests include diagnosis and prognosis for vehicle systems and machinery condition monitoring.

Chuanyan Xu received the Ph.D. degree in Vehicle Engineering from South China University of Technology, Guangzhou, P. R. China, in 2012. She is currently an associate professor of Vehicle Engineering in Shandong Jiaotong University. Her current research interests include diagnosis and prognosis for vehicle systems and machinery condition monitoring.